Ab Initio Study on the Substituent Effect in the Transition State of Keto−Enol Tautomerism of Acetyl Derivatives

Chen-Chang Wu and Min-Hsiung Lien*

Department of Chemistry, National Chung Hsing University, Taichung 402, Taiwan, Republic of China

Received: June 12, 1995; In Final Form: October 3, 1995[⊗]

Ab initio molecular orbital calculations have been performed on the intramolecular tautomerism of some acetyl derivatives, CH_3COX (X = H, BH_2, CH_3, NH_2, OH, F, Cl, CN, NC). All stationary points and the keto, enol, and transition structures were optimized at the HF/6-31G* and MP2(full)/6-31G* levels of theory and confirmed by frequency calculations. Single-point calculations at MP4(FC)/6-311++G**//MP2(Full)/6-31G* were also carried out for all stationary points. The intrinsic reaction coordinate (IRC) for the tautomeric processes were traced to connect the transition structures and the corresponding substituted tautomeric pairs. The natural bond orbital (NBO) analyses on the transition states show that the interactions of the lone pair electrons on the oxygen atom and the σ^* C−H bonds have a significant effect on their stabilities, which consequently affects the activation energies of the tautomeric processes. The energy barriers calculated at various levels of theory are reported for each tautomeric interconversion.

Introduction

Tautomerism is a prototropic rearrangement in which a hydrogen at the α-position to a carbon−heteroatom double bond migrates to the heteroatom and forms a C−C double bond. The tautomeric interconversions, e.g. keto ⇌ enol, imine ⇌ enamine, nitro ⇌ acinitro, nitroso ⇌ oxime, have been extensively studied both experimentally and theoretically. Among these rearrangements, the most investigated and documented are the keto/enol tautomeric pairs. The keto tautomers are generally lower in energy than their enol counterparts by roughly 20 kcal/mol in terms of bond energies,[1] indicating that the tautomeric equilibrium keto ⇌ enol lies heavily to the keto side. The prototype of the keto/enol tautomerism is the pair of acetaldehyde and vinyl alcohol:

$$\underset{\mathbf{1}}{H_3C(CO)H} \underset{\text{ketonization}}{\overset{\text{enolization}}{\rightleftharpoons}} \underset{\mathbf{2}}{H_2CCHOH} \qquad (1)$$

Vinyl alchol is a reactive intermediate formed in the pyrolysis of cyclobutanol.[2]

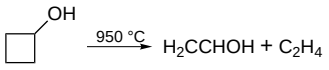

(2)

It has a half-life of 30 min, before rearranging to the more stable isomer, acetaldehyde. The decarboxylation of pyruvic acid also produces vinyl alcohol and acetaldehyde via the intermediary of a carbene, hydroxyethylidene.[3]

$$H_3C(CO)COOH \rightarrow CO_2 + H_3CCOH \rightarrow H_3C(CO)H + H_2CCHOH \quad (3)$$

Ab initio molecular orbtial calculations of the potential energy surface connecting the acetaldehyde and vinyl alcohol have been performed at various levels of theory.[4] At the "G1" level of theory, Radom et al. found vinyl alcohol **2** to lie 47 kJ/mol (11.2 kcal/mol) above **1** and to require 235 kJ/mol (56.2 kcal/mol) for conversion to acetaldehyde.

Although the thermodynamic stabilities of the keto/enol tautomeric isomers have been the subjects of experimental and theoretical investigation,[5] little has been done on the substituent effect and the kinetic aspects of the tautomeric equilibria. In view of the important role that the keto/enol tautomerism plays in various areas in chemistry, we have carried out high-level ab initio molecular orbital calculations on the acetyl derivatives

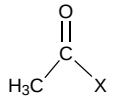

where X = H, BH_2, CH_3, NH_2, OH, F, Cl, CN, and NC, to study the effect of various substituents on the geometries and energetics of the keto and enol tautomers and on the transition states that interconnect them.

Computational Methods

Ab initio molecular orbital calculations employing both Hartree−Fock and Moller−Plesset perturbation theory at second-order (MP2)[6] levels of theory with the 6-31G*[7] basis set were carried out for all geometry optimizations. All calculated equilibrium structures (local minima and saddle points) of the keto and enol forms and the transition states connecting them were characterized by harmonic vibrational frequency calculations at the HF/6-31G* and MP2(Full)/6-31G* levels, which also furnished the zero-point vibrational energies (ZPVE) and other data. Intrinsic reaction coordinate (IRC)[8] calculations were performed to establish that the transition state was for the desired rearrangement. The natural bond orbital (NBO)[9] technique was applied to calculate the bond order,[10] which was used to analyze the nature of bonding in structures calculated for the stationary points at the HF/6-31G* level. To further correct for electron correlation, single-point calculations at the MP4(FC,SDTQ)/6-311++G** level based on the MP2(Full)/6-31G* optimized structures were also performed for all of the stationary points. The Gaussian90[11] and Gaussian92[12] package programs have been used throughout this work.

Results and Discussion

The potential energy profile for the interconversion of the substituted enol and keto tautomers is sketched in Figure 1.

[⊗] Abstract published in *Advance ACS Abstracts,* December 1, 1995.

0022-3654/96/20100-0594$12.00/0

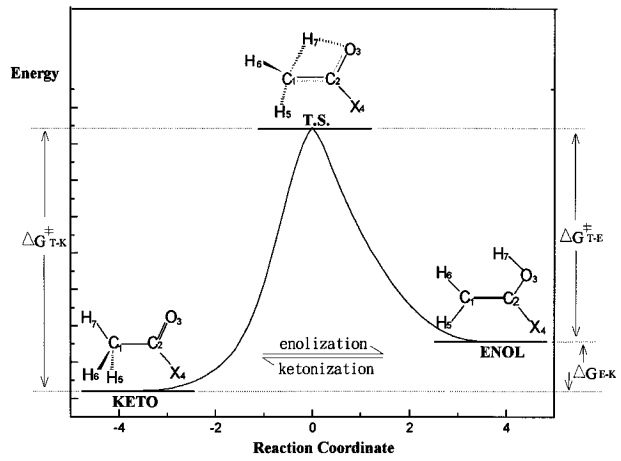

Figure 1.

Table 1 presents the geometric parameters of the optimized structures for the transition states connecting the keto and enol tautomers at both the HF/6-31G* and MP2(Full)/6-31G* levels of theory, while their total energies and zero-point vibrational energies at various levels of theory are reported in Table 2. With a few exceptions, the HF/6-31G* geometries generally reproduce the trends of the MP2(Full)/6-31G* results. Unless specifically noted otherwise, only the results based on the MP2(Full)/6-31G* calculations will be discussed. The complete set of optimal geometric parameters of all stationary points (in **Z**-matrix form), the bond orders from the natural bond calculations, and the Mulliken and natural population analyses are all available in the supporting information.

I. Keto and Enol Forms. As our main interest in this study lies in the substituent effect on the transition states and the activation energies in the tautomeric rearrangements, this report will focus on the results that are related to the transition structures.

In this section we shall not present a detailed discussion of the results from the calculations of the keto and enol tautomers for the sake of conciseness. However, the optimized structures at the HF/6-31G* and MP2(Full)/6-31G* levels of theory for the tautomers are depicted in Figure 2 along with the transition structures connecting them.

II. Transition Structures. *A. Geometric Parameters*. There are seven geometric parametes in Table 1 (namely, the bond lengths C_1-H_7, O_3-H_7, C_2-O_3, C_1-C_2, and C_2-X_4, the bond angle $H_7-C_2-C_1$ (the best parameter to present the reaction coordinate), and the dihedral angle $H_7-C_2-C_1-O_3$) that are of most interest and relevance to the tautomeric interconversion. We will discuss these parameters in detail here.

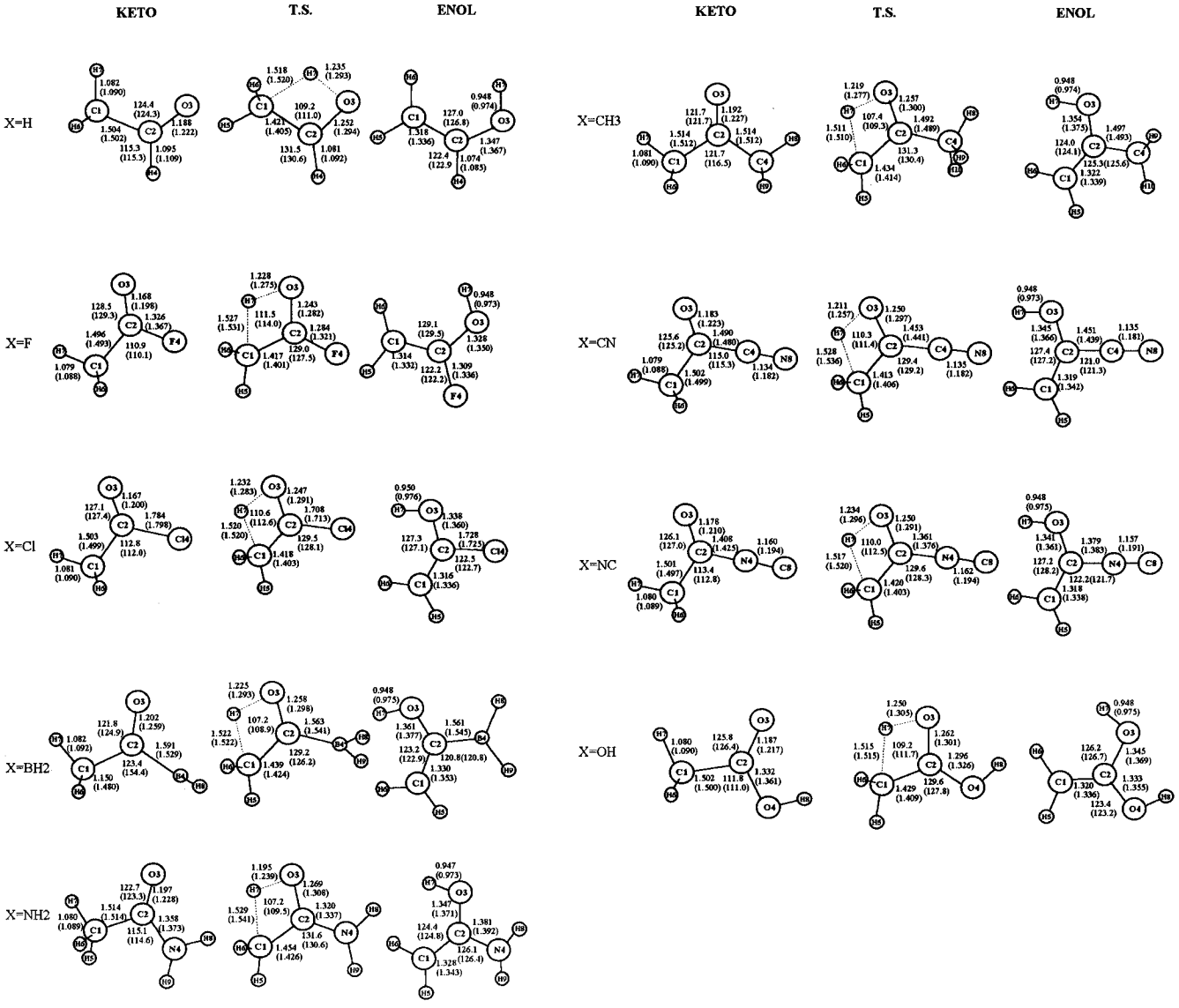

Figure 2. HF/6-31G* and MP2(Full)/6-31G* (in parentheses) optimized geometries for the keto, transition states, and enol forms.

TABLE 1: Geometric Parameters[a] of the Transition States

	X																	
	H		F		Cl		OH		CN		NC		BH_2		NH_2		CH_3	
parameters	HF	MP2	HF	MP2	HF	MP2	HF	MP2	HF	MP2	HF	MP2	HF	MP2	HF	MP2	HF	MP2
C_1-C_2	1.421	1.405	1.417	1.401	1.418	1.403	1.429	1.409	1.413	1.406	1.420	1.403	1.439	1.424	1.454	1.426	1.434	1.414
C_1-H_5	1.079	1.086	1.076	1.084	1.076	1.084	1.077	1.084	1.076	1.086	1.077	1.085	1.081	1.088	1.082	1.087	1.080	1.087
C_1-H_6	1.085	1.091	1.081	1.088	1.083	1.089	1.083	1.088	1.083	1.091	1.083	1.090	1.086	1.091	1.085	1.089	1.085	1.091
C_1-H_7	1.518	1.520	1.527	1.531	1.520	1.520	1.515	1.515	1.528	1.536	1.517	1.520	1.522	1.522	1.529	1.541	1.511	1.510
C_2-O_3	1.252	1.294	1.243	1.282	1.247	1.291	1.262	1.301	1.250	1.297	1.250	1.291	1.258	1.298	1.269	1.308	1.257	1.300
C_2-X_4	1.081	1.092	1.284	1.321	1.708	1.713	1.296	1.326	1.453	1.441	1.361	1.376	1.563	1.541	1.320	1.337	1.492	1.489
O_3-H_7	1.235	1.293	1.228	1.275	1.232	1.283	1.250	1.305	1.211	1.257	1.234	1.296	1.225	1.293	1.195	1.239	1.219	1.277
$X_4-(N_8,C_8,H_8)$							0.953	0.979	1.135	1.182	1.162	1.194	1.184	1.191	0.996	1.010	1.081	1.090
X_4-H_9													1.184	1.191	0.992	1.008	1.085	1.094
X_4-H_{10}																	1.085	1.093
$O_3-C_2-C_1$	109.2	111.0	111.5	114.0	110.6	112.6	109.2	111.7	110.3	111.4	110.0	112.5	107.2	108.9	107.2	109.5	107.4	109.3
$X_4-C_2-C_1$	131.5	130.6	129.0	127.5	129.5	128.1	129.6	127.8	129.4	129.2	129.6	128.3	129.2	126.2	131.6	130.6	131.3	130.4
$H_5-C_1-C_2$	120.7	121.7	119.7	120.4	120.4	121.2	118.8	119.9	121.3	121.8	120.3	121.3	120.4	121.7	117.9	119.5	121.1	121.3
$H_6-C_1-C_2$	110.0	112.9	110.8	113.8	110.2	113.3	110.0	112.9	110.5	113.0	110.3	113.2	109.8	112.5	109.3	112.0	109.6	112.7
$H_7-C_2-C_1$	60.1	60.2	61.7	62.5	61.0	61.4	61.0	62.0	60.3	60.1	60.6	61.0	59.3	59.0	60.1	61.2	59.4	59.5
$H_8-X_4-C_2$							110.0	107.6					118.7	119.1	120.3	120.0	111.5	111.4
$H_9-X_4-C_2$													119.4	119.7	120.8	120.9	109.1	109.5
$H_{10}-X_4-C_2$																	109.1	109.2
$X_4-C_2-C_1-O_3$	−177.2	−178.1	−174.4	−174.5	−175.6	−176.3	−174.7	−174.6	−177.5	−179.1	−176.2	−177.0	−181.4	−185.4	−176.3	−175.3	−177.6	−178.9
$H_5-C_1-C_2-O_3$	152.4	153.6	153.2	154.5	153.3	154.1	153.4	155.2	152.1	152.3	152.8	153.3	148.3	148.0	148.2	152.5	153.1	154.7
$H_6-C_1-C_2-O_3$	−73.7	−65.3	−71.6	−62.5	−71.4	−63.1	−74.6	−64.7	−70.8	−64.9	−72.2	−63.8	−79.0	−71.3	−83.3	−70.9	−75.2	−65.7
$H_7-C_2-C_1-O_3$	−7.9	−9.8	−9.6	−12.1	−9.1	−11.6	−9.4	−12.1	−8.4	−9.9	−8.8	−10.8	−6.9	−8.6	−7.9	−11.0	−8.2	−10.4
$H_8-X_4-C_2-O_3$							−4.9	−8.0					73.4	61.1	−4.3	−7.7	−10.3	−17.8
$H_9-X_4-C_2-O_3$													50.4	237.5	174.7	168.8	111.2	103.6
$H_{10}-X_4-C_2-O_3$																	−132.0	−139.1

[a] Bond distances in angstroms; bond angles and dihedral angles in degrees.

TABLE 2: Energetics of the Stationary Points

X	HF[a]	ZPVE[b]	T.E.[c]	S[d]	MP2[a]	ZPVE[b]	T.E.[c]	S[d]	MP4[a]
				Keto					
H	−152.915 97	37.68	40.10	62.84	−153.358 97	35.77	38.20	62.74	−153.495 06
F	−251.798 47	38.35	40.94	66.55	−252.413 3	31.57	34.25	67.13	−252.606 93
Cl	−611.831 20	32.06	34.83	69.42	−612.418 63	30.48	33.33	69.96	−612.583 32
OH	−227.810 65	42.77	45.58	68.11	−228.433 98	39.63	42.45	68.26	−228.618 80
CN	−244.642 15	37.21	40.43	72.06	−246.373 45	34.72	38.08	73.07	−245.541 42
NC	−244.629 86	36.85	40.19	72.87	−245.344 56	34.68	38.12	73.63	−245.518 22
BH_2	−178.160 27	41.95	45.62	75.42	−178.683 36	43.34	46.54	69.85	−178.842 64
NH_2	−207.976 01	49.56	52.73	71.30	−208.584 99	47.16	50.37	73.08	−208.765 15
CH_3	−191.962 24	56.49	59.69	69.38	−192.540 87	53.96	57.29	72.40	−192.718 78
$CH_3(CH_2)_4$	−348.102 13	133.20	139.57	101.44	−349.224 34				
C_6H_5	−382.476 37	93.04	97.64	85.62	−383.700 87				
				Enol					
H	−152.888 89	36.23	38.54	61.30	−153.332 16	38.29	38.29	61.03	−153.474 28
F	−251.746 56	33.28	35.72	65.08	−252.359 04	33.64	33.64	65.86	−252.559 72
Cl	−611.786 48	32.16	34.78	67.86	−612.371 79	32.80	32.80	68.44	−612.541 81
OH	−227.754 19	41.39	44.16	66.84	−228.375 80	41.42	41.42	68.51	−228.569 13
CN	−244.616 98	37.68	40.68	70.02	−245.347 95	37.85	37.85	70.99	−245.521 34
NC	−244.592 79	37.22	40.33	70.68	−245.308 64	37.79	37.79	71.51	−245.487 87
BH_2	−178.143 57	39.81	42.94	69.39	−178.662 29	46.21	46.21	68.87	−178.828 43
NH_2	−207.925 82	49.87	52.69	67.06	−208.533 91	49.83	49.83	68.11	−208.722 48
CH_3	−191.932 34	57.18	60.07	67.75	−192.511 65	57.22	57.22	68.52	−192.695 65
$CH_3(CH_2)_4$	−348.071 04	133.95	139.98	96.67	−349.194 44				
C_6H_5	−382.442 89	93.19	97.66	84.29	−383.672 38				
				T.S.					
H	−152.770 82	33.45	35.52	59.95	−153.237 71	32.37	34.43	59.98	−153.381 29
F	−251.639 90	29.05	31.40	64.58	−252.275 22	27.89	30.22	64.59	−252.477 15
Cl	−611.675 50	27.50	30.00	67.28	−612.285 78	26.78	29.27	67.21	−612.458 22
OH	−227.659 67	37.63	40.13	65.25	−228.301 97	35.94	38.39	64.97	−228.496 32
CN	−244.492 57	33.43	36.30	69.40	−245.250 86	31.19	34.17	70.13	−245.425 69
NC	−244.478 26	33.04	36.05	70.28	−245.215 31	31.14	34.19	70.61	−245.396 56
BH_2	−178.028 04	41.94	44.89	68.11	−178.569 84	39.17	42.14	68.17	−178.737 27
NH_2	−207.840 44	46.87	49.56	66.38	−208.466 94	43.74	46.50	66.72	−208.655 23
CH_3	−191.820 52	50.89	53.86	68.64	−192.421 37	50.47	53.45	69.48	−192.607 09
$CH_3(CH_2)_4$	−347.960 41	129.48	135.50	97.61	−349.104 89				
C_6H_5	−382.338 03	89.11	93.47	83.59	−383.587 28				

[a] In hartrees. [b] Zero-point vibrational energies in kcal/mol. [c] Thermal energies in kcal/mol. [d] Entropy in cal/(mol K).

On going from the keto forms to the transition states, the C_1-H_7 bond lengths increase by an average of 0.434 Å (0.441 Å at HF/6-31G*), while on going from the enol forms to the transition states, the O_3-H_7 bond lengths increase by an average of 0.306 Å (0.277 Å at HF/6-31G*). As is shown in Table 1, the inclusion of electron correlation has little effect on the C_1-H_7 bond lengths in the transition structures since their tendency toward lengthening in the HF/6-31G* calculations was virtually reproduced in the MP2/6-31G* calculations. The average bond length of C_2-O_3 is shortened from 1.361 Å in the enol forms to 1.296 Å in the transition states and then to 1.216 Å in the keto forms. It is seen that the MP2(Full)/6-31G* results are longer than those of the HF/6-31G* by an average of 0.033 Å in the transition structures. Conversely, the C_1-C_2 bonds are lengthened from an average of 1.338 to 1.08 Å (1.319 to 1.426 Å at HF/6-31G*) as the hydrogen migrates away from the oxygen atom in the enols to the transition states. As is shown in Figure 3, the C_2-X_4 distances (with the exception of the parent molecule, X = H) are the shortest in the transition structures. We will discuss this geometric parameter in more detail in section III. The average $H_7-C_2-C_1$ bond angle is 60.99°, as compared to that of 60.52° from the HF/6-31G* calculations. This also parallels the general trends of the MP2-(Full)/6-31G* calculations very closely. Finally with reference to the dihedral angles $H_7-C_2-C_1-O_3$, it is seen that the four-membered rings of the transition structures are very close to being planar, as the dihedral angles are found to be in the range 8.6−12.2° (6.9−9.6° at HF/6-31G*). It is of interest to note that the electron correlation affects the planarity of the four-membered ring, as it is observed that in all cases the MP2-(Full)/6-31G* values for this dihedral angle are larger than the HF/6-31G* ones by roughly 2°.

B. Bond Order. The calculated data at the HF/6-31G* level of theory show that the changes in bond orders are matched by the changes in bond lengths in Table 1 during the processes of ketonization and enolization. The lengthening of the bonds couples with the lowering of bond orders and vice versa. The average bond orders of the C_1-C_2 (1.265) and C_2-O_3 (1.371) bonds in the transition structures show that these bonds are intermediate between single and double. The C_1-H_7 bond orders, averaging 0.360, are larger than those of O_3-H_7 by 0.036. The natural bond orbital calculations also show that the O_3-H_7 bonds are not strongly held, as there is no two-center bond orbital observed, although some electron density is found to exist between O_3 and H_7.

C. Population Analysis. Several interesting observations emerge from the Mulliken population analysis (MPA)[13] and natural population analysis (NPA):[14] (1) In all cases the atomic charges obtained in NPA are larger than those from MPA. (2) In both analyses, the methylene carbons (C_1) carry the most negative charge, while the carbonyl carbons are the most positively charged centers, with the exception of X = H and X = Cl in MPA. (3) On going from the enol forms to the transition states, the migrating hydrogens carry about half of the net atomic charge along the reaction path.

D. $n_{O3} \rightarrow \sigma^*_{C1-H7}$ Interaction. The $n_{O3} \rightarrow \sigma^*_{C1-H7}$ interaction takes place when the lone pair electrons of the oxygen atom (n_{O3}) delocalize into the antibonding orbital (σ^*) of C_1-H_7:

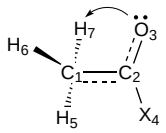

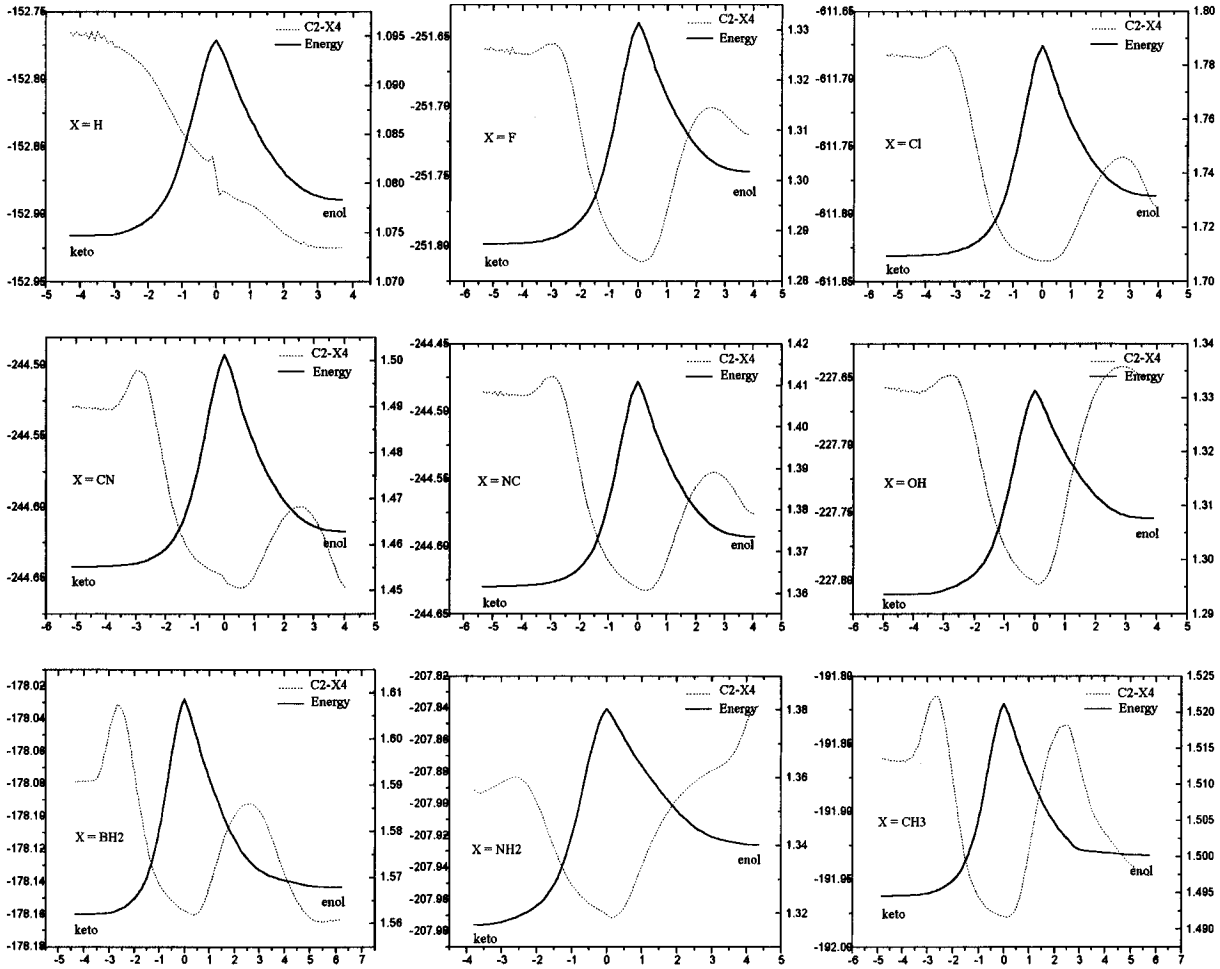

Figure 3. IRC plots of the total energies (solid lines, in hartrees) and the C_2-X_4 bond distances (dotted lines, in angstroms) versus reaction coordinates.

TABLE 3: Quantity of Charge Transfer (QCT)[a] between n_{O3} and σ^*_{C1-H7} of the Transition States

	X								
	H	F	Cl	OH	CN	NC	BH_2	NH_2	CH_3
QCT	0.33	0.30	0.30	0.35	0.28	0.29	0.34	0.37	0.34

[a] In au.

Table 3 shows that the transition structures with π-donating substituent groups have a larger quantity of charge transfer (QCT)[15] than those with π-accepting substituents. This is achieved by donating the electron density to O_3 via C_2. The $n_{O3} \rightarrow \sigma^*_{C1-H7}$ interaction has the following influences on the transition states: (1) increases the electron-withdrawing abilities of the oxygen atoms and the positive charge on the carbonyl carbon; (2) forms the π-electron-deficient center ($C_2{=}O_3$) and enhances the π-electron delocalization effect between the deficient center and substituent group; (3) shortens the bond length and increases the bond order of C_2-X_4 in the transition states compared with those in the keto and enol forms, as shown in Figure 3.

III. Intrinsic Reaction Coordinates. The reaction paths for the nine tautomeric processes were followed by means of the intrinsic reaction coordinate (IRC) calculations at the HF/6-31G* level. In Figures 1, 3, 5, 6, and 7, the transition structures are assigned to zero (at the center) on the reaction coordinate, with the keto forms at the minimum on the left and the enol forms on the right. It is seen that in all cases the keto tautomers are lower in energy than their enol counterparts with respect to relative energy, $\Delta G_{enol-keto}$ ranging from 13.18 kcal/mol (X = BH_2) to 35.40 kcal/mol (X = OH). To prove the link between the transition states and the corresponding keto and enol forms, we have performed IRC calculations on each tautomeric process at the HF/6-31G* level of theory. The computed energy profiles are shown in Figure 3. Here we will report more results from some selected IRC calculations for different probings. The dotted line and dot-dashed line in Figure 5 display the C−C and C−O bond lengths and total energy, respectively, for X = H. It is seen that on going from the keto forms to the enol forms, the C−C single bond in the former becomes a double bond in the latter. The converse is true for

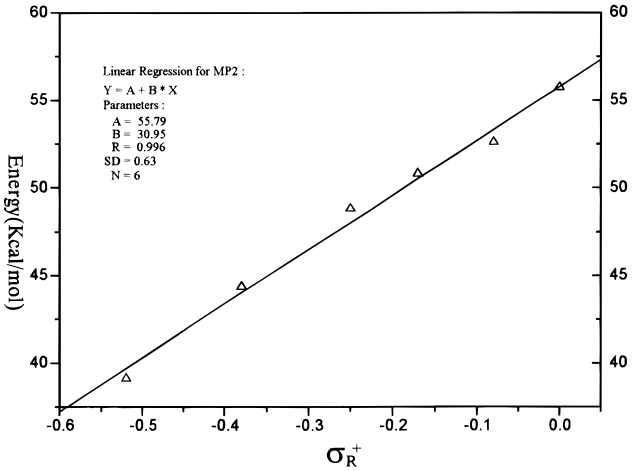

Figure 4. Barriers to ketonization versus the Hammett substituent resonance parameters: (Δ) the $\Delta G^{\ddagger}_{T-E}$ at MP2/6-31G*.

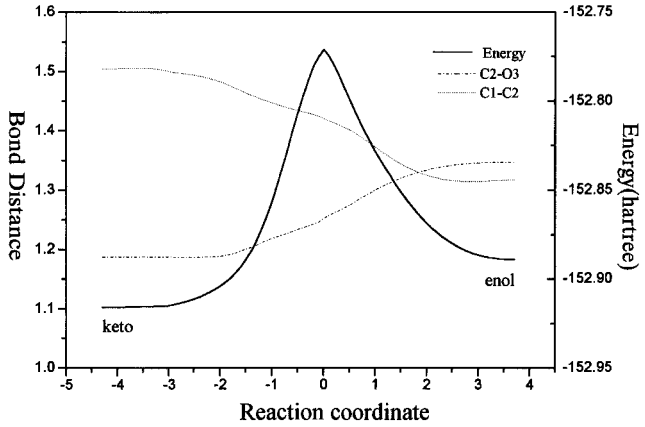

Figure 5. Bond length and the total energy versus reaction coordinate for X = H.

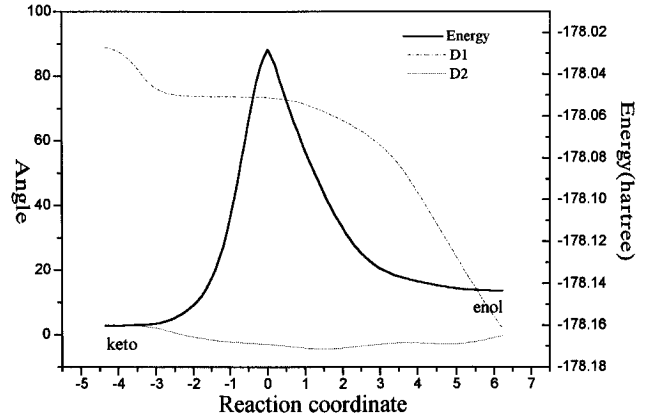

Figure 6. Dihedral angle and energy versus reaction coordinate for X = BH_2. D1 is the dihedral angle H8−B4−C2−O3; D2 is the dihedral angle (H8−B4−C4−H9 − 180).

the C−O bond throughout the enolization. It is found, although not shown here, that the rest of the tautomers follow the same trend that the parent tautomers (X = H) do in the tautomeric processes. Among the substituents, BH_2 and NH_2 have strikingly different characters in terms of the nature of the electron pair. The former is an electron deficient group with an empty p-atomic orbital on boron, whereas the latter has a lone-pair of electrons. Shown in Figure 6 are the two dihedral angles which characterize the BH_2 group in tautomeric processes. It can be seen that the dihedral angle $H_8-B_4-C_2-H_9$ remains consistently close to 180° along the reaction coordinate, implying that the BH_2 group maintains the sp^2 hybridization throughout the intramolecular tautomerism. Meanwhile the dihedral angle $H_8-B_4-C_2-O_3$ changes slowly from ∼90° in the first half of

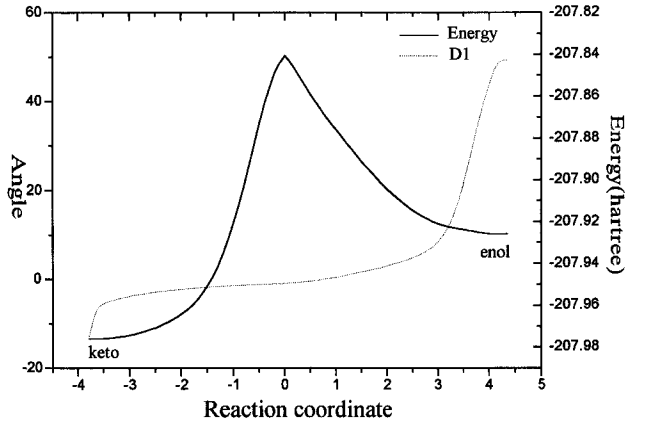

Figure 7. Dihedral angle and energy versus reaction coordinate for X = NH_2. D1 is the dihedral angle (H8−N4−C2−H9 − 180).

enolization and then rapidly to ∼0° toward the end. This observation suggests that the BH_2 group plays a dual role in going from the keto form to the enol form. Through hyperconjugation it acts as a π-donor during the first half along the reaction path and then becomes a π-acceptor in the second half. Finally with X = NH_2, we note in Figure 7 that on the path between the keto form and transition state, the amino group appears to have sp^2 hybridization and to react as a π-donor. As the enolization nears completion, the hybrid orbital changes from sp^2 to sp^3.

IV. Barriers to Ketonizations and the Resonance Effect. Table 2 shows that in all cases the keto tautomers are thermodynamically more stable than their enol counterparts at all levels of theory. The barriers to ketonization range from 39.1 kcal/mol (X = NH_2) to 57.5 kcal/mol (X = CN) compared with 50.7−73.9 kcal/mol and 39.3−56.6 kcal/mol at HF/6-31G* and MP4(FC)/6-311++G**//MP2(Full)/6-31G*, respectively. As expected, electron correlation lowers the energy barrier to the tautomeric interconversion by 11.5−16.4 kcal/mol at the MP2(Full)/6-31G* level and 11.4−17.3 kcal/mol at the MP4-(FC)/6-311++G** level.

The data in Table 4 show that the magnitude of the energy barrier to the ketonization varies with the electronic nature of the substituent group and is in the order

$$CN > H > NC > BH_2 > CH_3 > Cl > F > OH > NH_2$$

which is the same as that from the MP4(FC)/6-311++G**//MP2(Full)/6-31G* calculations. The HF/6-31G* calculations follow the trend of the results at higher levels of theory except for switching of the positions of Cl and CH_3. Analysis of the barrier to interconversion suggests that the substituents with

TABLE 4: Gibbs Free Energies (kcal/mol) and the Hammett Substituent Resonance Parameters σ_R^+

	HF/6-31G*			MP2/6-31G*			MP4/6-311++G**			
X	$\Delta G^‡$ T.S.−enol	$\Delta G^‡$ T.S.−keto	ΔG enol−keto	$\Delta G^‡$ T.S.−enol	$\Delta G^‡$ T.S.−keto	ΔG enol−keto	$\Delta G^‡$ T.S.−enol	$\Delta G^‡$ T.S.−keto	ΔG enol−keto	σ_R^{+d}
H	71.47	87.36	15.89	55.72	73.14	17.42	54.81	68.44	13.64	0.00
F	62.76	90.55	27.79	48.80	81.88	33.08	48.01	76.65	28.64	−0.25
Cl	65.03	93.51	28.48	50.81	80.12	29.32	49.29	75.26	25.97	−0.17
OH	55.76	90.14	34.39	44.35	79.76	35.40	43.71	73.78	30.06	−0.38
CN	73.87	90.53	16.65	57.50	73.89	16.39	56.60	69.59	12.99	0.00[a]
NC	67.71	91.76	24.06	55.23	78.08	22.84	53.97	73.31	19.35	−0.02[b]
BH_2	74.83	84.42	9.60	54.15	67.34	13.18	53.34	62.22	8.88	−0.05[b]
NH_2	50.65	83.37	32.72	39.11	72.10	33.00	39.28	67.00	27.72	−0.52
CH_3	63.69	83.32	19.63	52.60	72.02	19.42	51.52	67.12	15.60	−0.08
$CH_3(CH_2)_4$	64.66	86.00	21.34	51.71[c]	70.89	19.17				−0.07
C_6H_5	61.82	83.24	21.43	49.21[c]	67.05	17.84				−0.22

[a] This value is believed to be inaccurate; see ref 18. The calculated value is 0.06 from eq 4. [b] Calculated value. [c] Thermal energies at the HF/6-31G* level used; the calculated values are 53.62 and 48.98. [d] From ref 18, Table IX.

π-donating capacity or lone-pair electrons (e.g. F, OH, NH_2) tend to stabilize the transition structures and therefore lower the energy barrier to the ketonization. On the basis of the observation that the migrating H_7 atoms carry about half of the net atomic charge and the π-deficient C_2 atom resonates with the substituents in the ketonization, it is reasonable to use the resonance parameters, σ_R^+, for proton transfer in the gas phase compiled by Taft et al.[16,17] to correlate the activation energies and the resonance effect of the substituents.

We have examined the correlation using the empirical equation

$$\Delta G^{\ddagger} = A + B\sigma_R^+$$

where $\Delta G^{\ddagger}$ is the energy barrier and the σ_R^+ is the Hammett substituent resonance parameter[18] (see Table 4). Figure 4 shows the plots of the linear regressions for the linear equations:

at the MP2 level: $$\Delta G^{\ddagger} = 55.79 + 30.95\sigma_R^+ \qquad (4)$$

($n = 6$, $r = 0.996$).

We have excluded the substituents CN, NC, and BH_2 in the linear regressions because the reported resonance parameter for CN is considered to be unreliable[18] and those for NC and BH_2 are not available. Our calculations indicate that eq 4 best represents the linear relationship between $\Delta G^{\ddagger}$ and σ_R^+ and is therefore used to obtain the calculated σ_R^+ of 0.06, -0.02, and -0.05 for X = CN, NC, and BH_2, respectively. To check whether (4) also holds for other substituents, we have included X = $CH_3(CH_2)_4$ and C_6H_5 in this study. Using the σ_R^+ data of Taft et al. in (4), the $\Delta G^{\ddagger}$ for X = $CH_3(CH_2)_4$ and C_6H_5 are predicted to be 53.62 and 48.98 kcal/mol, respectively. These are in good agreement with the MP2(Full)/6-31G*//MP2(Full)/6-31G* values of 51.7 and 49.2 kcal/mol. This accord allows us to place confidence in the applicability of (4).

Conclusion

On the basis of our work, we summarize the following conclusions.

(1) The tautomeric interconversions of the acetyl derivatives are 1,3 hydrogen positive ion shift processes. The substituents with π-donating ability tend to have a lower energy barrier.

(2) Thermodynamically, the keto tautomers are more stable than their enol counterparts.

(3) A linear relationship in the form of $\Delta G^{\ddagger} = 55.79 + 30.95\sigma_R^+$ at the MP2 level between the Gibbs free energy of ketonization and the Hammett substituent resonance parameters exists.

(4) The calculated barriers are all rather high and would indicate only slow interconversions. The lower barrier suggested by experiment may result from catalysis by acidic or basic impurities or by bimolecular reactions.

Acknowledgment. The continued financial support of the National Science Council of the Republic of China is gratefully acknowledged. We are indebted to the National Center for High-Performance Computing for a generous allocation of SRU on the CONVEX C3840. We thank Professors A. C. Hopkinson and Andrew Streitwieser for many helpful discussions.

Supporting Information Available: The geometry structures of all stationary points (in **Z**-matrix form), the bond orders, and the population analysis (20 pages). Ordering information is given on any current masthead page.

References and Notes

(1) Lovering; Laidler. *Can. J. Chem.* **1960**, *38*, 2367.

(2) (a) Saito, S. *Chem. Phys. Lett.* **1976**, *42*, 399. (b) Rodler, M.; Bauder, A. *J. Am. Chem. Soc.* **1984**, *106*, 4025.

(3) Saito, K.; Sasaki, G.; Okada, K.; Tanaka, S. *J. Phys. Chem.* **1994**, *98*, 3756−3761.

(4) (a) Bouma, W. J.; Poppinger, D.; Radom, L. *J. Am. Chem. Soc.* **1977**, *99*, 6443. (b) Kunttu, H.; Dahlqvist, M.; Murto, J.; Räsänen, M. *J. Phys. Chem.* **1988**, *92*, 1495. (c) Smith, B. J.; Radom, L.; Kresge, A. *J. Am. Chem. Soc.* **1989**, *111*, 8297. (d) Smith, B. J.; Radom, L. *J. Am. Chem. Soc.* **1990**, *112*, 7525. (e) Apeloig, Y.; Arad, D.; Rappoport, Z. *J. Am. Chem. Soc.* **1990**, *112*, 9131. (f) Wiberg, K. B.; Breneman, C. M.; LePage, T. J. *J. Am. Chem. Soc.* **1990**, *112*, 61. (g) Smith, B. J.; Nguyen, M. T.; Bouma, W. J.; Radom, L. *J. Am. Chem. Soc.* **1991**, *113*, 6452.

(5) (a) Shainyan, B. A.; Mirskova, A. N. *Russ. Chem. Rev.* **1979**, *48*, 107. (b) Hart, H. *Chem. Rev.* **1979**, *79*, 515. (c) Capon, B.; Guo, B. Z.; Kowk, F. C.; Siddhanta, A. K.; Zucco, C. *Acc. Chem. Res.* **1988**, *21*, 135. (d) Rappoport, Z.; Biali, S. E. *Acc. Chem. Res.* **1988**, *21*, 422. (e) Heinrich, N.; Koch, W.; Frenking, G.; Schwarz, H. *J. Am. Chem. Soc.* **1986**, *108*, 593. (f) Chiang, Y.; Kresge, A. J.; Schepp, N. P. *J. Am. Chem. Soc.* **1989**, *111*, 3977. (g) Akao, K.; Yoshimura, Y. *J. Chem. Phys.* **1991**, *94*, 5243. (h) Correa, R. A.; Lindner, P. E.; Lemal, D. M. *J. Am. Chem. Soc.* **1994**, *116*, 10795. (i) Francis, J. T.; Hitchcock, A. P. *J. Phys. Chem.* **1994**, *98*, 3650. (j) Saunders, W. H. *J. Am. Chem. Soc.* **1994**, *116*, 5400. (k) Bernasconi, C. F.; Wenzel, P. J. *J. Am. Chem. Soc.* **1994**, *116*, 5405.

(6) (a) Moller, C.; Plesset, M. S. *Phys. Rev.* **1934**, *46*, 618. (b) Pople, J. A.; Binkley, J. S.; Seeger, R. *Int. J. Quantum Chem., Symp.* **1976**, *10*, 1. (c) Krishnan, R.; Pople, J. A. *Int. J. Quantum Chem.* **1978**, *14*, 91.

(7) (a) Hariharan, P. C.; Pople, J. A. *Theor. Chem. Acta* **1973**, *28*, 213. (b) Francl, M. M.; Pietro, W. J.; Hehre, W. J.; Binkley, J. S.; Gordon, M. S.; Pople, J. A. *J. Chem. Phys.* **1982**, *77*, 3654.

(8) Gonzalez, C.; Schlegel, H. B. *J. Chem. Phys.* **1989**, *90*, 2154.

(9) (a) NBO Version 3.1, Glendening, E. D.; Reed, A. E.; Carpenter, J. E.; Weinhold, F. (b) Foster, J. P.; Weinhold, F. *J. Am. Chem. Soc.* **1980**, *102*, 7211. (c) Reed, A. E.; Weinhold, F. *J. Chem. Phys.* **1983**, *78*, 4006. (d) Reed, A. E.; Weinstock, R. B.; Weinhold, F. *J. Chem. Phys.* **1985**, *83*, 735. (e) Carpenter, J. E.; Weinhold, F. *J. Mol. Struct.* **1988**, *169*, 41. (f) Reed, A. E.; Curtiss, L. A.; Weinhold, F. *Chem. Rev.* **1988**, *88*, 899.

(10) Wiberg, K. *Tetrahedron* **1968**, *24*, 1083.

(11) Frisch, M. J.; Head-Gordon, M.; Trucks, G. W.; Foresman, J. B.; Schlegel, H. B.; Raghavachari, K.; Robb, M.; Binkley, J. S.; Gonzalez, C.; Defrees, D. J.; Fox, D. J.; Whiteside, R. A.; Seeger, R.; Melius, C. F.; Baker, J.; Martin, R. L.; Kahn, L. R.; Stewart, J. J. P.; Topiol, S.; Pople, J. A. *Gaussian 90*, Revision J; Gaussian, Inc.: Pittsburgh, PA, 1990.

(12) Frisch, M. J.; Trucks, G. W.; Head-Gordon, M.; Gill, P. M. W.; Wong, M. W.; Foresman, J. B.; Johnson, B. G.; Schlegel, H. B.; Robb, M. A.; Replogle, E. S.; Gomperts, R.; Andres, J. L.; Raghavachari, K.; Binkley, J. S.; Gonzalez, C.; Martin, R. L.; Fox, D. J.; Defrees, D. J.; Baker, J.; Stewart, J. J. P.; Pople, J. A. *Gaussian 92*, Revision C.4; Gaussian, Inc.: Pittsburgh, PA, 1992.

(13) Mulliken, R. S. *J. Chem. Phys.* **1955**, *23*, 1833.

(14) See ref 9c,d.

(15) See ref 9f.

(16) Taft, R. W.; Topsom, R. D. *Prog. Phys. Org. Chem.* **1987**, *16*, 1.

(17) Taft, R. W.; Koppel, I. A.; Topsom, R. D.; Anvia, F. *J. Am. Chem. Soc.* **1990**, *112*, 2047.

(18) Hansch, C.; Leo, A.; Taft, R. W. *Chem. Rev.* **1991**, *91*, 165.

JP951647M